A Physical Mooring Comparison for a Floating OWC

Keri Collins [#1], Ben Howey[#], Pedro Vicente[*2], Rui Gomes[†3], Violette Harnois[‡], Martyn Hann[#], Gregorio Iglesias[#], Deborah Greaves[#4]

[#] *School of Engineering, Plymouth University, Drake Circus, Plymouth, UK, PL4 8AA*

[1]keri.collins@plymouth.ac.uk, [4]deborah.greaves@plymouth.ac.uk

[*] *WavEC, Rua Dom Jerónimo Osório, 11,1 º, 1400-119, Lisbon, Portugal*

[2]pedro.vicente@wavec.org

[†] *IDMEC, Instituto Superior Técnico, Universidade de Lisboa Av. Rovisco Pais, 1049-001 Lisbon, Portugal*

[‡]*INNOSEA, 1 rue de la Noë, 44321 Nantes, France*

Abstract— **A physical comparison of a single isolated Spar Buoy type oscillating water column with two mooring types was carried out in Plymouth University's Coast Laboratory. A simple catenary chain solution was compared to a hybrid line with floats and sinkers. The effect on performance via a decoupled motion analysis, as well as mooring tension was investigated. Results indicated a performance improvement can be made through the use of hybrid moorings.**

Keywords— Moorings, Survivability, Performance, Hybrid mooring, Catenary

I. Introduction

In order to propel the wave energy sector to a commercial state, WETFEET was set up under the EU's Horizon 2020 Framework Programme. A significant area highlighted as requiring progression is array architecture that will be explored as part of work package 6 of the project [1]. The axisymetric floating spar buoy oscillating water column (OWC), developed by the Instituto Superior Técnico in Lisbon, was selected as the energy converter for physical testing. This device consists of a hollow tail tube attached to a float that, when excited by a wave field, drives air through the tube and subsequently, an air turbine [2].

It has been shown in many works [3] that the mooring system of any motion dependant wave energy converter (WEC) is an integral part of the energy extraction device that needs to be considered at an early design stage. Further, it has been identified that in order to push wave energy towards commercialization, devices will need to be arranged in farm configurations to maximize the output [4]. The nature of closely packed arrays means that the total array power can be greater than the sum of the power resultant from the same number of isolated devices [5]. As a result, it is often beneficial to moor devices in close proximity to one another. Mooring configurations can become an issue when simple chain catenary systems cross one another owing to the array configuration. It is hypothesized that the restoring forces of a simple catenary can be matched with a hybrid system that has a smaller length of line on the seabed. With less line on the seabed, devices can be moored closer together without the risk of line interaction. Reduced seabed interference is also a positive factor for an array's environmental impact. It is further proposed that the horizontal restoring forces can be matched, while allowing motion along the vertical axis of the device, thus improving power output, as found in [6].

II. Methodology

The spar buoy used in this investigation, shown in Figure 1, is a 1:40 scale model of the OWC design that has been developed by IST [2], [7], [8]. At full scale, the spar buoy has a total length of 50 m and designed to work as a floating off-shore OWC. The widened end of the bottom tube shown in Figure 1 was designed to increase the mass of the device without changing its hydrostatic characteristics, which allows more flexibility in tuning the device to the incoming wave conditions [9]. At full scale, the natural heave frequency of the device is 1.43 Hz (0.697 Hz at 1:40 scale) and the water column has a natural frequency of 1.79 Hz (0.558 Hz at 1:40 scale).

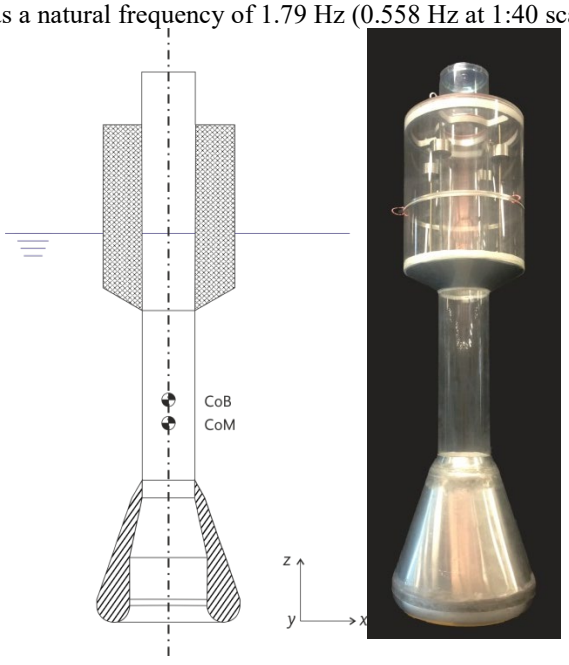

Figure 1 Section view of the proposed spar buoy geometry (left) and the 1:40 model built for the experiments (right).

In the full-scale embodiment of the spar buoy, the power take-off (PTO) mechanism is envisaged to be an impulse turbine. Orifice plates are used to simulate mass flow rates proportional to the square of the pressure difference [10]. In keeping with previous work undertaken on this design [8], an orifice plate 15% of the OWC tube diameter was chosen to provide the PTO damping in the scale model experiments.

A. Catenary Design

A catenary mooring made solely from chain was used as a benchmark for the restoring characteristics for the hybrid system to approximate. Figure 2 shows the form of a catenary mooring. The total length of the mooring, L, extends from the anchor point to the WEC with a portion resting on the sea floor and the free-floating length given by L_s.

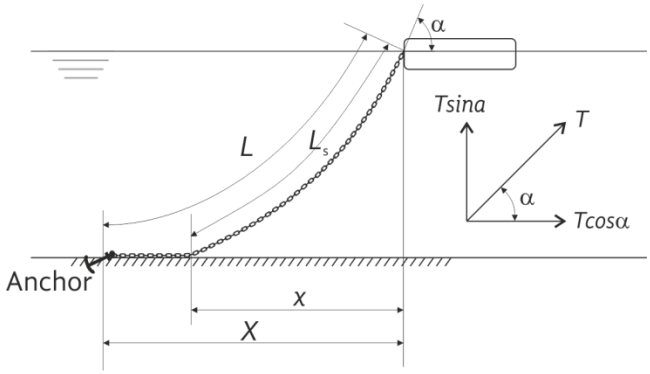

Figure 2 Dimensions of a catenary design.

The horizontal distance between the anchor and the WEC, X, and between the touchdown point of the chain and the WEC, x, can be used with the inelastic quasistatic equations, (1) and (2), to calculate the chain length, L, and its weight.

$$X = L - L_s + x \tag{1}$$

$$X = L - z\left(1 + 2\frac{a}{z}\right)^{\frac{1}{2}} + a \cdot cosh^{-1}\left(1 + \frac{z}{a}\right) \tag{2}$$

Where a is the quotient of the horizontal tension, T_h, and the chain weight per unit length in air, w. The horizontal tension was calculated by assuming the restoring horizontal tension from the catenary to be equal and opposite to the maximum expected loading from wind, current and wave forces acting on the device [11].

A chain was chosen to withstand the tensions with a safety factor of 1.7, in accordance with DNV-OS-C101 for quasistatic approaches [12]. The selected chain had an associated weight per unit length that was used in the catenary equations to calculate the length required at full scale. The dynamic effect of the chain was assessed in OrcaFlex using a vessel and 6 degree of freedom (dof) buoy model with hydrodynamic coefficients calculated in WAMIT.

It was not possible to acquire a chain that matched the scaled-down wet weight per unit length. Instead, the dimensions of the chain were scaled, Table I, and a commercially available chain with the closest bar diameter was selected for the experiments. The wet weight per unit length of the model-scale chain was calculated based on the dry mass per unit length and the published value of the material density. As a result, the model-scale chain was found to be ≈16% lighter in water than the theoretical value.

TABLE I
SCALED AND ACHIEVED CATENARY CHARACTERISTICS.

Characteristic	Full Scale	1:40 Scale Theoretical	Achieved
Mooring radius [m]	210	5.25	5.25
Length (L_s) [m]	240	6.00	6.00
Chain diameter [mm]	180	4.50	4.00
Wet weight per unit length [N/m]	4800	3.00	2.51

B. Hybrid Line Design

Figure 3 shows the hybrid line components. The inclusion of clump weights and floats enables the footprint on the seabed of the system to be minimized while providing similar restoring characteristics to that of the catenary. Unlike a catenary, this allows for lines to easily pass under one another. Initially a quasistatic approach was taken to design the hybrid line. Similar to [9], static equilibrium conditions were computed numerically by solving the system of non-linear equations generated from the geometric and equilibrium of force constraints.

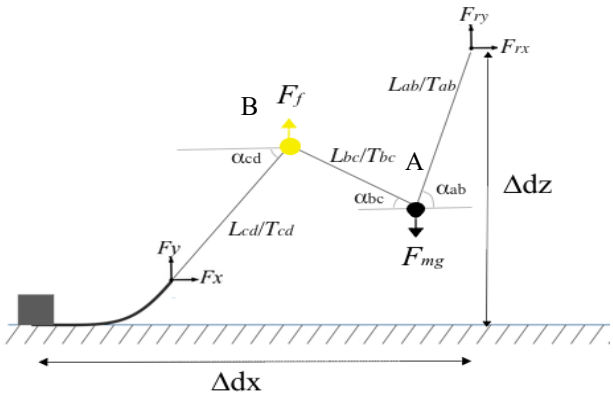

Figure 3 Dimensions and angles of the hybrid line.

Equations (3) and (4) equate the force in the x direction at the clump weight (A) and the float (B) respectively and the forces in the y direction at the same points are considered in (5) and (6). Two geometric constraints related to the total x and y lengths of the whole system are applied with Equations (7) and (8).

$$\sum F_{xA}\ 0 = T_{ab}\cos(\alpha_{ab}) - T_{bc}\cos(\alpha_{bc}) \tag{3}$$

(4)

$$\sum F_{xB}\ 0 = T_{bc}\cos(\alpha_{bc}) - T_{cd}\cos(\alpha_{cd}) \tag{5}$$

(6)

$$\sum F_{yA}\ 0 = T_{ab}\sin(\alpha_{ab}) + T_{bc}\cos(\alpha_{bc}) - F_{mg} \tag{7}$$

$$\sum F_{yB}\, 0 = F_f - T_{bc}\sin(\alpha_{bc}) - T_{cd}\cos(\alpha_{cd}) \tag{8}$$

$$\Delta dx = L_{ab}\cos(\alpha_{ab}) + L_{bc}\cos(\alpha_{bc}) + L_{cd}\cos(\alpha_{cd}) + acosh^{-1}\left(1+\frac{h}{a}\right)$$

$$\Delta dx = L_{ab}\sin(\alpha_{ab}) + L_{bc}\sin(\alpha_{bc}) + L_{cd}\sin(\alpha_{cd}) + h$$

The line lengths, mass and float size that produced restoring characteristics most similar to those of the chain-only configuration were selected. The dynamics of the system were analysed in OrcaFlex as this allowed for the effects of damping on the floats, masses and lines to be included in the solution.

The hybrid lines were constructed using ultra high molecular weight polyethylene (Dyneema) for the line sections, stainless steel chain for the lower catenary, lead for the clump weight and Styrofoam for the float sections. The Dyneema sections' lengths were scaled as shown in Table II. One piece of Dyneema was used for the three sections, reducing the number of joins in the line that could fail. The lines were tied to the fairleads and chain sections with bowlines.

To scale the components, the wet weights of the 1:40 scale (theoretical) components were matched so that the restoring characteristics remained constant. This took into account the change in water density and the change in the density between the materials proposed for the full-scale design and those available for the model. The clump weights were tied to the lines at a distance of L_{ab} from the fairlead and the total volume of foam was divided between six float units and threaded on to the lines with a small distance separating each float.

TABLE II
CHARACTERISTICS OF THE MOORING LINES

Characteristic	Full Scale	1:40 Scale - Theoretical	Achieved
Radius [m]	210.00	5.25	5.25
L_{ab} [m]	51.56	1.29	1.29
L_{bc} [m]	21.81	0.55	0.55
L_{cd} [m]	127.10	3.18	3.18
Clump mass [kg]	129066.71	2.02	1.81
Clump density [kg/m^3]	5600	5600	11340
Float mass [kg]	326.80	0.0051	0.0011
Float density [kg/m^3]	150	150	35

C. Basin and model set up

The spar buoy model (hence device) was moored with three equiangular lines that connected the model at approximately the still water level. The three lines were anchored to the bottom of the University of Plymouth Ocean Basin as shown in Figure 4, with centre of the device approximately coincident with the geometric centre of the basin. The mooring lines were rotated with respect to the basin axes such that the downstream line rotated 5.15° from the *x*-axis. To correspond to the chosen full-scale location of the Leixões, Portugal, for which the offshore water depth is 80 m, the floor of the Ocean Basin was set at 2 m water depth.

Using the basin coordinate system given in Figure 4, the movement of the device is defined. The three translations: surge, sway and heave are motions along the *x*, *y*, and *z* axes respectively. Similarly, the rotations: roll, pitch and yaw are positive rotations about these axes such that a positive roll would indicate the top of the device moving towards mooring Line 3.

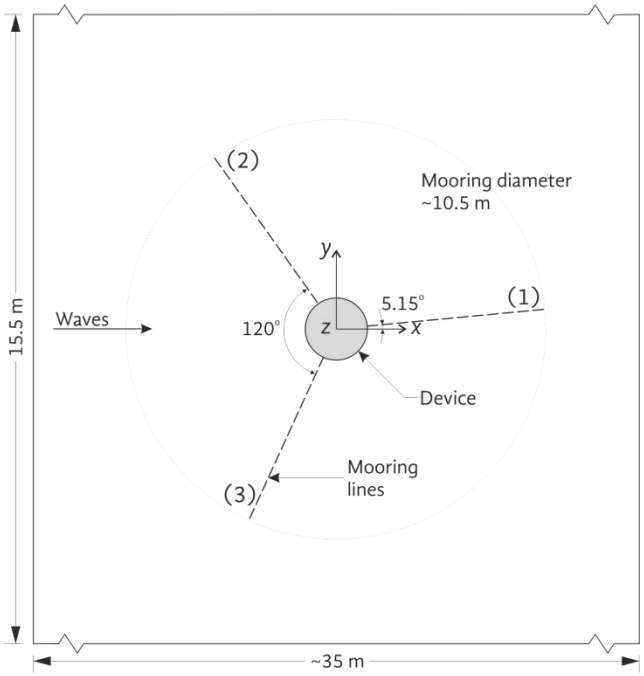

Figure 4 – Set up of the device and the mooring lines in the University of Plymouth Ocean Basin. Waves travel in the +x direction towards a parabolic dissipative beach (not shown). The water depth was 2 m.

Figure 5 shows an underwater view of both mooring conditions taken from the –*x* (upstream) side of Line 3. The toe of the beach is visible in the background. The hybrid mooring line was designed to be used in a close-spaced array of devices; by having a touchdown point closer to the anchor, Figure 5, the hybrid lines from an array of devices would be able to cross without touching.

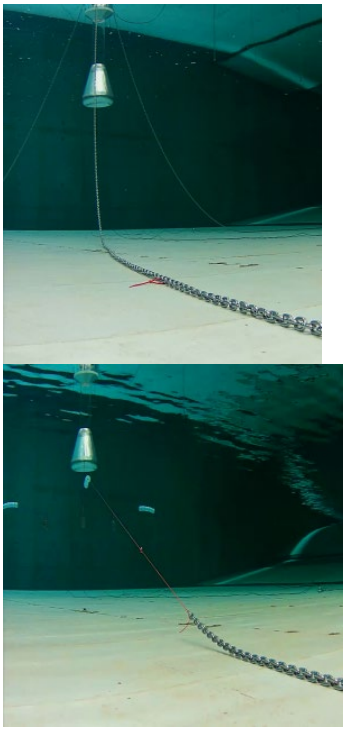

Figure 5 Underwater images of the catenary (left) and hybrid line mooring (right) in the University of Plymouth Ocean Basin.

D. Wave Climate

Regular waves of 0.2 m wave height (H=8 m at full scale) were used to analyse the performance, and survivability cases were used to analyse the loading on the different mooring systems. Irregular and survivability waves were modelled as Pierson-Moskovitz spectra. The survivability cases were calculated from the linear transformation of the Weibull distribution of wave heights from the Ondatlas Mar3G numerical model. A linear regression model was used to extrapolate the probabilities to that of a 10-year return period. The significant wave height, H_s, and peak period, T_p, associated with the 50-year return period were H_s = 0.3 m and T_p = 2.72 s at 1:40 scale.

E. Measurements and data analysis

Incident waves were measured with nine resistive wave gauges placed around the basin for the empty basin condition as well as for the two moored device cases. A zero-crossing method was used to determine the average properties of the regular waves and the incident wave power was calculated using $P = \frac{\rho g H^2}{8} c_g$, where ρ is the water density, g is the acceleration due to gravity, H is the wave height and c_g is the group celerity.

The volumetric flow rate through an orifice is a quadratic function of the chamber pressure and hence the mean power will be proportional to the mean pressure raised to the power of 3/2. Typically for wave energy, the capture width, defined as the ratio of converted power to the power per metre of incident wave crest, is used to describe the power production. A differential pressure sensor (Honeywell, HSCSAAN010NDAA5) was attached to the orifice plate of the device with one port measuring the internal chamber pressure and the other port open to atmospheric pressure. Voltage readings were converted to pascals. At the time of experiments, the orifice had not been calibrated and so results reported in Section III describe the pseudo capture width. In this paper, we have made this dimensionless by normalizing by the maximum capture width found in all tests, as in [13].

S-beam load cells (Futek, LSB210) were located between each of the lines and the fairleads of the device to measure the line tension. The zero-load offset of each load cell was subtracted from the results and the still water reading was noted as the value of pre-tension in the mooring lines.

Small retroreflective markers were placed on the top of each device and the six degree of freedom (6 dof) motion data was captured using an infrared camera-marker system (Qualisys).

Surface elevation data were recorded at 128 Hz using the basin control software (Edinburgh Designs Ltd). The 6 dof motion data were recorded at 128 Hz using the Qualisys software and the load cells and pressure sensors were recorded at 1667 Hz using a bespoke LabVIEW program. Data acquisition was synchronised at the start of each experiment.

III. Results

The objective of the experiments was to determine the effect of the two mooring types on device performance and survivability. Decay tests were carried out in order to determine any change to the heave natural frequency due to the mooring systems. The performance was quantified using the measurement of the chamber pressures and the 6 dof motion of the buoys. Force sensors placed at the fairleads of the mooring lines were used to assess the survivability.

We concentrate on the heave of the device as other motions of the device have previously been found to be uncoupled to the turbine damping, which plays a major role in the performance [9].

Since the experiments were part of a larger project, in total 6 spar buoy devices were built. Results are presented for the model shown in Figure 1, with additional data associated with one other model presented for the decay tests. The difference in the spar buoy models and the implications for the results is discussed in Section IV.

A. Decay Tests

Displacement and release decay tests were performed for the chain mooring and the hybrid mooring. The device moored with chains was depressed in the water manually and the 6 dof motion tracking system was used to record the motion of device. For the hybrid mooring system, a second spar buoy model was used for the decay test and the model was raised in heave by means of a line and pulley arrangement. Each decay test was repeated to give three data for each mooring.

Figure 6 shows the motion of the device during one moored heave decay test. It can be seen that towards the end of the experiment, the heave oscillations were not as consistent in size or period, in particular for the hybrid mooring line. Exponential curves were fitted to different numbers of peaks and troughs of the data, varying from 3–10, and the RMSE between the data and the fit was calculated. The RMSE was at a minimum when only 3 data were used, so the first three oscillations were used to determine the natural heave frequency of the moored devices. The mean of three tests was taken and showed that the natural frequency of the chain mooring system was $f_{cha} = 0.657$ Hz whereas for the hybrid system it was $f_{hyb} = 0.675$ Hz. The relevance of this apparent difference in natural heave frequency, and the influence of the models themselves, is discussed in Section IV.

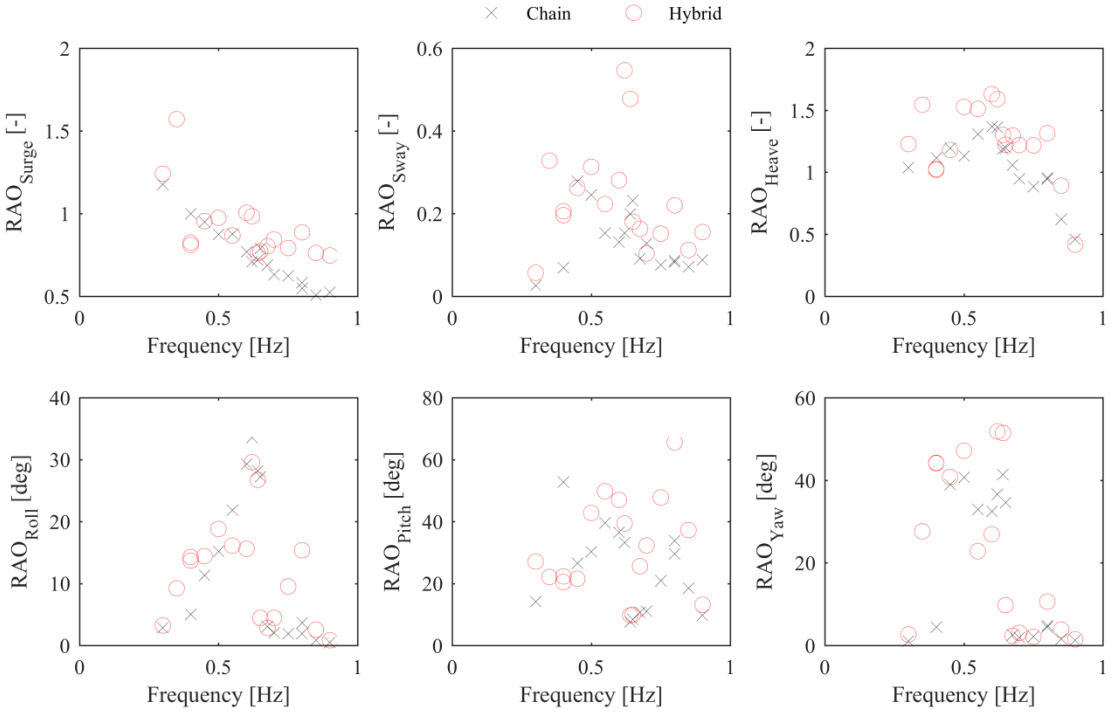

Figure 7 Motion response in all six degrees of freedom for the catenary and hybrid line configurations

B. Motion Response

Figure 7 shows the response amplitude operators (RAO) for each of the six degrees of freedom as a function of wave frequency. The RAO is the ratio of the magnitude of the response motion to that of the driving motion, here the wave height, and so for the translations the RAO is dimensionless.

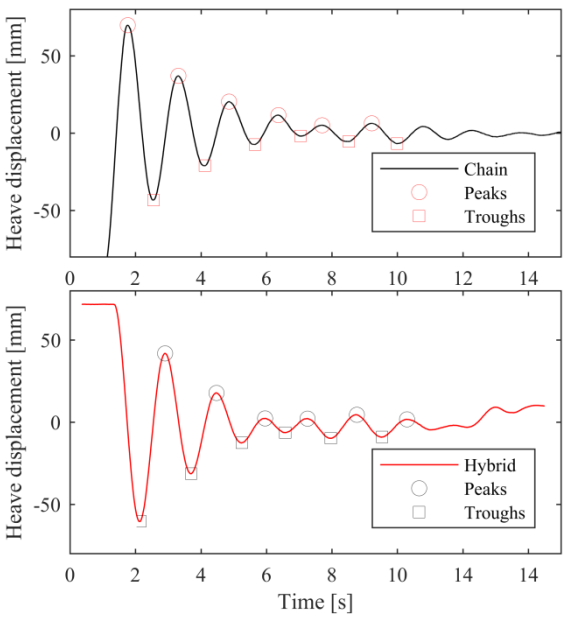

Figure 6 Heave decay test results for the chain and hybrid line mooring

For the rotations, the response units are different to those of the driving motion, thus the rotational RAO is given in degrees per metre. Figure 7 shows that the surge responses of the hybrid and the catenary lines were similar, with the hybrid line providing slightly less of a restoring force at many of the frequencies. The sway results for both lines were smaller than that of the other translational modes, with the hybrid line again providing slightly less of a restoring force. The most important response with respect to performance is the heave response and Figure 7 indicates that the hybrid line allowed a larger heave response, with no apparent shift of the peak circa 0.65 Hz. On inspection of the rotational modes, the hybrid line seemed to allow a greater response in all modes. The pitch showed a resonant peak around 0.8 Hz with a maximum value double that of the yaw response and 25% more than the roll.

C. *Line Tensions*

The power spectral densities of the line tensions for both mooring types are shown in Figure 8. These were computed with a fast Fourier Transform with the Welch method to smooth the outputs. The three vertical dotted lines on the Figure indicate the incident spectrum peak frequency, the theoretical natural frequency of the OWC and the theoretical natural frequency of the unmoored device.

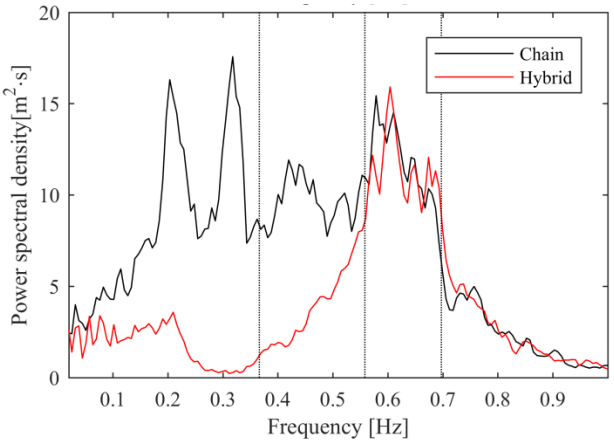

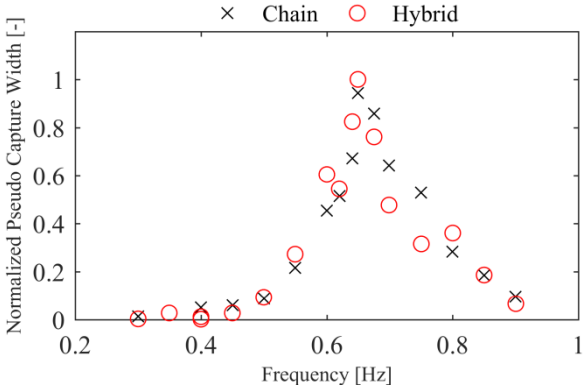

Figure 10 Dimensionless capture width plotted against frequency at constant amplitude of incident wave.

Figure 8 Spectral responses of the tension of in Line 2 of each of the mooring systems. From left to right, the three vertical lines indicate the peak frequency of the input spectrum and the theoretical natural frequencies of the water column and the unmoored device.

The tension in the chain showed a fairly broad-banded result but with large peaks at approximately 0.20 Hz and 0.32 Hz, and with smaller peaks at 0.43 Hz and 0.58 Hz. In contrast, there was no energy in the tension spectrum for the hybrid mooring at a frequency of 0.3 Hz, with a gradual rise up to the peak at $f \approx 0.6$ Hz.

Line tension time series indicated that Line 2 suffered from the highest loading conditions in both the hybrid and chain mooring case. Similar to that found in [14],a peak over threshold analysis (POT) was used to investigate the difference in each case [14]. The pre-tension was removed to assess the cyclic nature of the loading and a threshold of 3.8 N was selected. The number and magnitude of the peaks are represented in Figure 9 in which the two highest loads (22 N and 46 N) were recorded for the chain mooring.

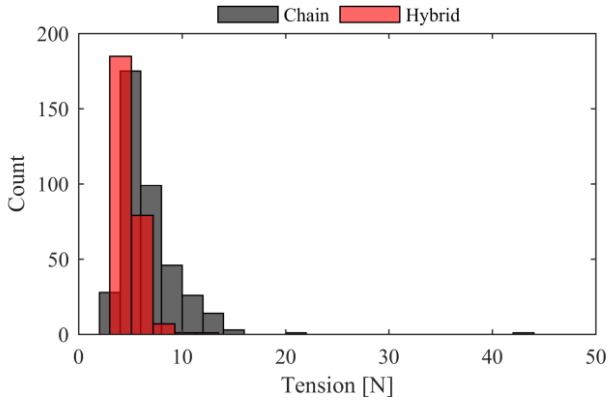

Figure 9 A histogram of the peaks over a 3.8 N threshold in a 10-year extreme sea state for the chain and hybrid mooring

It can be seen that the magnitude of the peak tension in Line 2 of the chain mooring is approximately three times higher than that of the hybrid line. The higher number of peaks over the threshold also indicates that the probability of a tension spike over the threshold is also higher for the chain system. From examining the load cell data under no wave loading, it was clear that the hybrid line had a higher static tension.

D. *Dimensionless Pseudo Capture Width*

The heave motion should dominate the power response and given that the moored natural heave frequencies were similar, it may be expected that the two arrangements produce the same power. Figure 10 shows that the dimensionless pseudo capture width was similar for both mooring configurations across the range of frequencies tested. The peak performance was at $f \approx 0.65$ Hz for both arrangements although the chain mooring appears to cause a lower value of pseudo capture width. The hybrid line appears to produce lower pseudo capture width than the chain mooring after the peak up to around $f = 0.8$ Hz.

IV. Discussion

It was hypothesized that the restoring forces of a simple catenary can be matched with a hybrid system that has a smaller seabed footprint. The previous section showed that the two mooring systems produced similar motions of device and that the pseudo capture width for both sets of experiments was similar but the tension response of the two lines was quite different.

The decay tests showed that the natural heave frequency of the configurations was different (f_{cha} = 0.657 Hz compared to f_{hyb} = 0.675 Hz) but owing to the small number of data this was not a statistically significant difference. Since the form of the oscillations changed over time, being affected by motions in the other degrees of freedom, the number of oscillations included in the calculation of the damping and the natural frequency was low. For most of the tests, three oscillations were chosen since the sum of the root mean squared errors between the peaks and the exponential fit from the upper and lower peaks was at a minimum with three oscillations. Once the number of oscillations was chosen, the mean period and the frequency for those oscillations were calculated. Whilst there was a difference in the mean natural frequencies across three independent tests, due to the lack of data, the difference between the two was not statistically significant. With so few oscillations available for the calculation of the natural frequency, it is recommended that the decay tests are repeated to give at least 10 independent tests.

The calculation of the natural frequency of the heave motion is further complicated by the use of two different models. Whilst the geometry of the two models was the same, the model used for the chain mooring decay test had a slightly lower mass. If modelled as a mass-spring-damper system, the moored spar buoy should have a higher natural frequency with a lower mass. The fact that the chain-moored model had a lower natural frequency with a lower model mass implies that the chain mooring did significantly lower the natural frequency of the heave motions.

The moored natural frequencies were lower than the unmoored design natural frequency of the device ($f_{nat, UD}$ = 0.697 Hz) and separate experiments showed that the measured unmoored heave natural frequency of the device used for the hybrid mooring decay tests was equal to $f_{nat, UM}$ = 0.693 Hz. Assuming the radiation damping from the device remained constant across both mooring configurations, the increased damping is assumed to stem from the mooring system. This is most likely owing to the added mass and viscous damping of the float and clump weights of the hybrid system.

Assuming the difference in the natural frequencies of the two device-mooring systems to be real, it is not discernible in the pseudo capture width or in the motion data. This implies that effect of a lower natural heave frequency is small compared to the other factors; both physical, such as the influence of the other motions, and experimental, such as the repeatability of the experiment.

The RAOs quantify the motion response of the device with respect to the incoming regular wave amplitudes. The heave response was amplified at the approximate value of the natural frequency of the moored configurations, although a difference between the RAO peaks from each configuration is hard to discern. A second peak in the heave RAO may be apparent at f = 0.8 Hz for both mooring systems and when compared to the pseudo capture width plot, Figure 10, a small rise in the hybrid mooring capture width is also apparent at this frequency. Repeated experiments may show that this is an artefact of one experiment. In separate (unreported) experiments, the 95% confidence interval of the pseudo capture width was approximately ±4% of the peak value.

The tension in the line can only come from the relative movement of the fairlead and the next component in the mooring line: the touchdown position of the chain in the case of the chain only and the clump weight for the hybrid line. Given that the device RAOs and the capture width were very similar, the large differences in the tension spectra are possibly due to the motion of the clump weight relative to the line fairlead.

With the current experiment it was not possible to determine the movement of the clump weight. It would be very interesting to examine the motion of the clump weight and to measure the tension at other points of the hybrid line. In addition, coupling the 6 dof motions of the device to the tension response would allow a more in depth analysis of the mooring line tension response. It may be that the anchor forces are lower for the hybrid line as energy is dissipated by the movement (and drag) of the clump weight.

The peaks over threshold analysis ignored the static tension on the lines; only the cyclic component of the load was considered. Despite the hybrid mooring having a higher pre-tension, the cyclic component of the load was similar for the chain and the hybrid mooring for the low loads. The chain mooring exhibited larger counts of larger cyclic loading components and some very large peak loads.

No analysis has yet been done on the loading time history and so the effects of the loads on the fatigue are unknown at this point; one method that has been suggested for this is a rainflow analysis. However, considering the results of the experiments here, the hybrid mooring had a higher pretension but a smaller range of dynamic loading. In terms of fatigue and indeed fatigue prediction, dynamic loads over a smaller range may be preferable to a high dynamic force range, even considering the lack of a knowledge base on synthetic lines [3]. In addition, a smaller dynamic force range should allow a more conservative safety factor to be employed, resulting in a potentially cheaper system.

V. Conclusions

In order to arrange arrays of wave energy converters, pure catenary chains are not always the most suitable option owing to water depths and mooring footprints. The use of hybrid lines including chain, rope, floats and clump weights make it possible to improve performance while reducing the line on the seabed. A physical comparison of a hybrid and chain catenary showed that small performance improvements can be made through the use of a hybrid mooring within certain frequency bandwidths. The greater benefit was noticed in the mooring

tension characteristics, where the cyclic loading magnitude on the hybrid lines was dramatically reduced, resulting in fatigue performance improvements vital to extend time between costly maintenance schedules at full scale.

The performance enhancements appear to be related to the reduced vertical restoring forces of the hybrid line, whilst the surge motions appear to be also slightly larger. These combined effects highlight the possibility for hybrid lines with float and clump sections to allow tightly packed device arrays without compromising performance or survivability.

ACKNOWLEDGMENT

This project has received funding from the European Union's Horizon 2020 research and innovation programme under grant agreement No 641334.

REFERENCES

[1] WETFEET, "WETFEET Project," 2015. [Online]. Available: http://www.wetfeet.eu/wetfeet-project/. [Accessed 09 December 2016].

[2] R. Gomes, L. Gato, A. Falcao, J. Henriques, P. Vicente, P. Ruiz-Minguela, Varandas, J. Varandas and L. Trigo, "Experimental Validation of a Spar Buoy Design for Wave Energy Conversion," Marinet, Lisboa, 2013.

[3] R. J. L. &. W. J. Harris, "Mooring systems for wave energy converters: A review of design issues and choices," in *3rd International Conference on Marine Renewable Energy*, 2004.

[4] P. Ricci, A. Rico, P. Ruiz-Minguela, F. Boscolo and J. Villate, "Design, Modelling and Analysis of an Integrated Mooring System for Wave Energy Arrays," Dublin, 2012.

[5] T. Weller and T. Stallard, "Float Response within an Array: Numerical and Experimental Comparison," Brest, 2008.

[6] J. Fitzgerald and L. Bergdahl, "Including Moorings in the Assessment of a Gneric Offshore Wave Energy Converter: A Frequency Domain Approach," vol. 21, no. 1, 2008.

[7] R. Gomes, J. Henriques, L. Gato and A. Falcao, "Hydrodynamic Optimization of an Axisymmetric Floating Oscillating Water Column for Wave Energy Conversion," *Renewable Energy,* vol. 44, no. 1, pp. 328-339, 2012.

[8] F. Fonseca, "Testing of a 1:32 scale model of a floating oscillating water column system for wave energy conversion," Instituto Superior Tecnico, Lisbon, 2015.

[9] R. Gomes, J. Henriques, L. Gato and A. Falcao, "Wave Channel Tests of a Slack-moored Floating Oscillating Water Column in Regular Waves," Nantes, 2015.

[10] A. Sarmento and A. Falcao, "Wave Generation by an Oscillating Surfacce-Pressure," *Fluid Mechanics,* vol. 150, pp. 467-485, 1985.

[11] L. Johanning, G. Smith and J. Wolfram, "Mooring design Approach for Wave Energy Converters," vol. 220, no. 4, 2006.

[12] DNV, "Design of Offshore Steel Structures, General (LRFD Method)," Det Norske Veritas, Oslo, 2011.

[13] A. Falcão, J. Henriques, R. Gomes, P. Vicente, F. Fonseca, J. Varandas and L. Trigo, "Dynamics of oscillating water column spar-buoy wave energy converters deployed in array and its survivability in extreme conditions," Marinet, Lisboa, 2015.

[14] V. Harnois, L. Johanning and P. Thies, "Wave Conditions Inducing Extreme Mooring Loads on a Dynamically Responding Moored Structure," Aalborg, 2013.

[15] A. Vickers and L. Johanning, "Comparison of Damping Properties for Three Different Mooring Arrangements," Uppsala, 2009.